Materials Chemistry and Physics 256 (2020) 123691

Contents lists available at ScienceDirect

Materials Chemistry and Physics

journal homepage: www.elsevier.com/locate/matchemphys

Metal telluride nanotubes: Synthesis, and applications

Raja Azadar Hussain [a,*], Iqtadar Hussain [b,*]

[a] Department of Chemistry, Quaid-i-Azam University, 45320, Islamabad, Pakistan
[b] Department of Mathematics, Statistics and Physics, Qatar University, Doha, 2713, Qatar

HIGHLIGHTS

- Synthetic methods of telluride nanotubes have been reviewed.
- Thermoelectric properties have been offered.
- Water splitting ability has been presented.

ARTICLE INFO

Keywords:
Metal tellurides
Nanotubes
Hydrothermal
Electrochemical

ABSTRACT

Metal tellurides have been explored extensively just like their sulfide and selenide cousins due to their surface chemistry, quantum confinement and physical properties. Nanotubular metal tellurides are more promising in terms of their unique physics and chemistry. This review article presents synthesis of metal telluride nanotubes via hydro/solvothermal methods, electrochemical methods, chemical methods, microwave methods and combination processes. Thermoelectric applications, electrocatalytic activities for water oxidation and supercapacitive behavior of metal telluride nanotubes have also been discussed and compared with other materials.

1. Introduction

Properties of materials can be controlled by controlling the sizes and shapes. As the size decreases, surface to volume ratio increases which imparts hybrid properties to the materials. These hybrid properties are different from bulk properties of same chemical composition. Shape on the other end determines the facets (reaction sites). Type and number of atoms on those facets are different for different morphologies. Metal chalcogenides are the combination of electropositive elements and groups VIA elements (sulfur, selenium and tellurium). Oxides are generally not discussed with chalcogenides. Metal chalcogenides have been under immense investigation as a reciprocal of noble metal materials such as platinum, rhodium, iridium, palladium and gold for device applications [1–6].

The fact that inorganic compounds can exist in the form of graphitic layers of formulae MX_2 (M = W, Mo, Nb, Hf and X = S, Se) [7] was known well before the discovery of carbon nanotubes [8]. In these compounds metal atoms are sandwiched between two chalcogen atoms layers with coordination number four (trigonal pyramidal) or six (octahedral) [9]. When these layers are observed from c-axis, dangling pattern is observed due to the absence of one metal or chalcogen atom at the edge. These dichalcogenide layers cannot bend like graphite but can roll into curved shapes. However first synthetic attempt of inorganic nanotubes was published in 1992 [10].

Metal tellurides are the chalcogenides which consist of tellurium as electronegative element with different electropositive metals. Tellurium, selenium and polonium are metalloid whereas sulfur and oxygen are nonmetals in oxygen family (16 A group of periodic table). These characteristic properties of elements in 16 A group play an important role for structural dependent applications of metal oxides, sulfides, selenides and tellurides. Metal tellurides have been synthesized via solid state metathesis [11], solvo (hydro)thermal methods [12], colloidal nonaqueous synthesis [13] and microwave assisted methods [14]. Low temperature synthesis helps to synthesize polytellurides which improve the morphology and crystal structure. Soft synthetic chemistry is important for the fabrication of desired low dimensional tellurides. Keeping synthetic methods on one side, concentrations of reactants (metal and tellurium) also play vital role for different dimensions of tellurides. In case of metal rich tellurides, metal-metal bonding extends to three dimensional network whereas tellurium rich tellurides have tellurium-tellurium extended structures to produce low dimensional tellurides with anisotropic physical properties [15]. Transition metal

* Corresponding authors.
E-mail addresses: hussainazadar@yahoo.com (R.A. Hussain), iqtadarqau@gmail.com (I. Hussain).

https://doi.org/10.1016/j.matchemphys.2020.123691
Received 29 May 2020; Received in revised form 26 July 2020; Accepted 13 August 2020
Available online 16 August 2020
0254-0584/

Table 1
Metal telluride nanotubes synthesized by different methods.

Material	Method	Precursors	Template	Temp (°C), time (h)	Additives	Ref.
Ag_2Te	Hydrothermal	Silver nitrate, sodium tellurate	nil	120, 12	hydrazine, ammonia	[46]
Ag_2Te	Electrospinning, Thermal reduction, Electrodeposition,	Silver nitrate, Tellurium	Ag nanofibers		polyvinylpyrrolidone	[67]
CdTe	Electrospinning, Electrodeposition, Cation exchange	Ag_2Te, cadmium nitrate	Ag nanofibers	50-90, 2	tributylphosphine	[65]
CdTe	DC-Electrodeposition	Cadmium sulfate, tellurium oxide, cadmium chloride	Anodic aluminum oxide	70, 1	nil	[58]
CdTe	Chemical	CdTe nanoparticles	nil	68, 1-6	thioglcolic acid, dodecanethiol	[60]
CoTe	Hydrothermal	Cobalt sulfate, tellurium oxide	Te nanorods (in situ)	180, 30	glucose, ethanol amine	[49]
CoTe and $CoTe_2$	Hydrothermal	Cobalt nitrate, H_2TeO_3	nil	140, 24-48	hydrazine	[51]
CoTe	Hydrothermal	Cobalt hydroxy carbonate film, Te powder	nil	90, 3 and 5	rongalite	[50]
$CoTe_2$	Solvothermal	Cobalt chloride, Te	Te NTs (in situ)	200, 24	oleic acid, ethylene glycol	[55]
In_2Te_3	Solvothermal	Sodium tellurate, Indium nitrate	nil	180, 48	polyvinylpyrrolidone, ethylene diamine	[56]
$MoTe_2$	Electron irradiation	Commercial $MoTe_2$				[95]
PbTe	Electrospinning, Electrodeposition, Cation exchange	Ag_2Te, lead nitrate	Ag nanofibers	4 h for cation exchange	tributylphosphine in cation exchange	[66]
Bi_2Te_3	Microwave assisted	Bismuth nitrate, tellurium oxide	nil	(180, 190, 195), 0.5–1	ethylene glycol	[64]
Bi_2Te_3	Hydrothermal	Bismuth chloride, Te powder	nil	67, 3.5 d	sdium borohydride, sodium hydroxide, EDTA	[54]
Bi_2Te_3	Chemical	Bismuth-TOPO, Te nanowires	Te nanowires	80-86, 12	trioctylphosphine oxide	[61]
Bi_2Te_3	Hydrothermal	Bismuth chloride, Sodium tellurate	nil	180, 48	EDTA, polyvinylpyrrolidone, sodium dodecyl sulfate, cetyltrimethyl ammonium bromide	[52]
Bi_2Te_3	Solvothermal	Bismuth chloride, Te powder	nil	140, 10-36	dimethyl formamide, Na-EDTA	[53]
Bi_2Te_3	Electrodeposition	Bismuth oxide, Tellurium oxide	polycarbonate		nitric acid (2 M)	[57]
Bi_2Te_3	Galvanic displacement	Bi^{3+},Te^{2+}	Ni NTs			[59]
Bi_2Te_3	Hydrothermal	Bismuth chloride, K_2TeO_3	nil	140, 1 week	polyvinylpyrrolidone	[71]
Bi_2Te_3	Chemical	Tellurium oxide, Bismuth nitrate	Te NRs	140-160, 0.5–1	polyvinylpyrrolidone, KOH, Ethylene glycol	[72]
Bi_2Te_3	Chemical	Bismuth nitrate, Tellurium oxide	Te NWs (in situ)	160, 1	ethylene glycol, polyvinylpyrrolidone, hydrazine	[62]
Sb_2Te_3	Microwave assisted solvothermal	Antimony chloride, Tellurium oxide	nil	200, 0.25	ethylene glycol, hydrazine	[68]
$Ni_{0.33}Co_{0.67}Te$	Solvothermal, cation exchange	$Ni(NO_3)_2{\cdot}6H_2O$, $Co(NO_3)_2{\cdot}6H_2O$, Na_2TeO_3	nil	120-180, 8-12	urea, nickel foam, hydrazine	[69]

(TM) tellurides which exist as clusters have triangular, tetrahedral and octahedral motifs. Poly tetrahedral clusters are exhibited by group 7 and 8 elements whereas poly octahedral structures are predominant for molybdenum tellurides (Mo_6Te_{14}) [16]. 1D motifs provide chains of $PtTe_2$ ribbons or PtTe zigzags separated by alkali metals [17]. With 1D motifs, fused octahedral chains have been observed for $K_4Ti_3Te_9$ [18], K_2ZrTe_3 [19] and $CsTaTe_3$ [20]. In 1D motifs category, tetrahedral chains exist via vertex sharing (Ba_2MnTe_3 [21], Ba_2CdTe_3 [22] and Ba_2HgTe_3 [15]) and edge sharing (K_2ZnTe_2 [23], K_2MnTe_2, Rb_2MnTe_2, and Cs_2MnTe_2 etc.) [24]. Other two classifications with 1D motif are layers having $TMTe_4$ tetrahedra ($K_2Cu_5Te_5$) [25] with Te–Te bonds and $TMTe_6$ octahedral layers ($LiTiTe_2$, $LiCrTe_2$ and NaCrTe) [26]. Due to large electronegativity of tellurium relative to sulfur and transition metals, its compounds are not electron deficient (except poly tellurides) and therefore low dimensional motifs prevail. 3D networks also exists ($Ba_3Cu_{13+x}Te_{12}$ and $Cs_3Cu_{20}Te_{13}$ and $K_4Ag_8Te_{11}$) [27,28] but mostly they may be broken down to simple repeating 1D structural motifs [15]. Metal tellurides have shown interesting optical, electrical and thermal properties [29] but work in this domain on nanotubular morphology is seldom reported.

Metal chalcogenides especially metal sulfides (copper sulfide [5,30,31], cobalt sulfide [32], nickel sulfide [33], zinc sulfide [34], manganese sulfide [35], cadmium sulfide [36] and silver sulfide [37]) and metal selenides (cadmium selenide [4], nickel selenide [2], copper selenide [3], iron selenide [38–43], manganese selenide [44,45] etc.) have been explored extensively with all the morphologies and sizes for water splitting, counter electrodes in solar cells, self repairable electrodes, thermoelectric properties, flexible electronics, fuel cells, photocatalysis, supercapacitors, chemical sensing and superconductivity. After such an extensive research, next logical goal was to check metal tellurides for same applications. Metal tellurides find applications in optoelectronics, photocatalysis, electrocatalysis and biology. Metal telluride nanomaterials have been reviewed in detail by Deepika Jamwal et al., in 2019 [29]. This review article discusses size controlled synthetic strategies, substantial properties and some applications of metal tellurides. Another important review article by Hayati Mamur et al. covers the synthesis and thermoelectric applications of bismuth telluride. To the best of our knowledge there is no review article which covers nanotubular morphology of metal tellurides specifically therefore in this review article we have covered all the synthetic approaches, applications and future horizons for this particular morphology.

2. Synthesis of metal telluride nanotubes

Metal telluride nanotubes have been synthesized over the years by using bottom up approach. Methods which have been used for synthesis

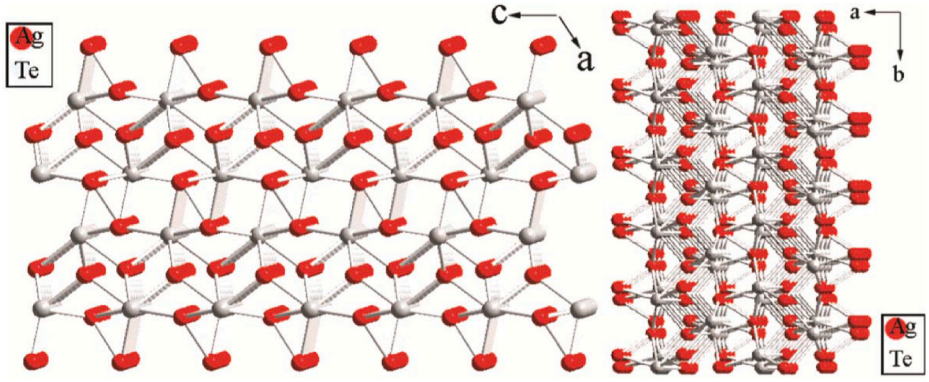

Fig. 1. Structure of β-Ag_2Te along b and c axes. Reproduced with permission from Refs. [46]. Copyright ACS 2007.

include hydrothermal method, solvothermal method, chemical method, electrodeposition, electronic irradiation method, microwave method and cation exchange method. During synthesis of metal telluride nanotubes, templates may be added as a reactant or they may be in situ produced. Template free synthesis of metal telluride nanotubes is also common due to their inherent structural rolling up capabilities. We shall now discuss the synthesis of metal telluride nanotubes by these methods one by one in detail below.

2.1. Hydrothermal method

Hydrothermal methods are widely used for the synthesis of metal chalcogenide nanostructures [1–4,32,35,36,38–43]. These methods are characterized by the mixing of reactants in water and carrying out the reaction inside a metallic autoclave. High temperature and pressure treatments generally increase the solubilities of reactant and they combine to form the desired products. To prevent the aggregation and agglomeration, surface active agents (ehylenediaminetetraacetic acid (EDTA), polyvinylpyrrolidone (PVP), trioctylphosphine oxide (TOPO), sodium dodecyl sulfate (SDS), cetyltrimethylammonium bromide (CTAB), ethylene glycol, ethylene diamine, tributyl phosphine (TBP), oleylamine (OlA) and oleic acid (OA)) may be added (Table 1). Ions of electropositive metals and electronegative tellurium show too much affinity for oxygen to form oxides. To avoid the impurity of oxygen in tellurides, reducing agents such as hydrazine and sodium borohydride are also used wherever required. Monoclinic β-Ag_2Te nanotubes were synthesized using hydrothermal method in the presence of ammonia (Table 1) [46]. Presence of ammonia is necessary for the formation of nanotubes in this study. If ammonia is not used then elemental Ag and Te are the products. In fact, ammonia forms a complex ($[Ag(NH_3)_2]^+$) with Ag^+ ions which hinder their reduction to metallic Ag before their reaction with Te. Formation of nanotubes proceeds by the formation of nanobelts at an early stage of reaction which are then changed to half tubes and then complete tubes [46]. To have a glimpse of growth mechanism, crystal structure of β-Ag_2Te was considered along b and c planes (Fig. 1). Ag (1) is tetrahedrally bonded to Te forming a sheet which is parallel to (100) plane. Similarly Ag (2) also forms a sheet which is linked to the fist sheet via two tetrahedral corners. These two layers roll up to form Ag_2Te nanotubes just like other natural and artificial lamellar solids [47,48].

In a very similar way hexagonal CoTe nanotubes of 80–120 nm diameter and 10–20 nm wall thickness (Fig. 2) were produced in a stainless steel autoclave with glucose and ethanol amine as additives (Table 1) [49]. Fig. 2b (inset) shows that the tubes are polycrystalline however they preferably grew along (210) direction. This (210) direction is at right angle to Te nanorods which served as templates. In the absence of glucose and keeping all the other conditions of reaction same, CoTe nanorods were produced. This means that ethanol amine can reduce TeO_2 to Te^{2-} which then reacts with cobalt to form CoTe nanorods. When 0.5 g of glucose is used in the reaction, CdTe nanotubes of 60 nm inner diameter are formed. By increasing the concentration of glucose to 1 g this average diameter reduces to 20 nm. So by changing the concentration of glucose, average internal diameter of CoTe nanotubes can be managed easily. Time resolved studies showed that at an early stage of reaction (1 h), Te nanorods are formed. When reaction is prolonged to 5 h these Te nanorods are converted to Te^{2-} anions. At third stage these anions react with Co^{2+} to form CoTe nanoparticles. Glucose in these reactions acted as a reducing agent which reduces TeO_2 to Te^{2-} or we should say it supports the reduction process. When Te nanorods are reduced they produce a vacancy for the induction of CoTe nanoparticles. With this successive addition of CoTe nanoparticles, CoTe nanotubes are formed along (210) plane [49]. Sometimes combination of methods is used to prepare the telluride nanotubes of desired composition and morphology. Kim et al. have synthesized cobalt hydroxyl carbonate films via hydrothermal method and then these films were immersed in Te precursor solution to have CoTe nanotubes thin films (Table 1) [50,51].

Effect of four different surface active agents EDTA, PVP, SDS and CTAB have been monitored for hydrothermal synthesis of Bi_2Te_3 in different experiments. Only EDTA produces the nanotubular morphology. Reason lies in multidentate donation sites of EDTA which may form different types of multinuclear bismuth complexes which are linked with each other via hydrogen bonding to produce lamellar moieties. These lamellar moieties then decompose in specialized manner during hydrothermal treatment to form the nanotubes [52]. When reactants ($BiCl_3$, Na_2TeO_3 and EDTA) are mixed together, complexation of bismuth ions takes place with EDTA. Remaining bismuth ions will slowly react with Te ions to start the nucleation of Bi_2Te_3. At 180 °C these nuclei are converted to nanoflakes with defects in their crystal structure. These defects twist the flakes into spirals which then generate the nanotubes [52]. Similar results have been obtained for solvothermal synthesis of Bi_2Te_3 in the presence of EDTA–Na salt [53]. Some other workers have synthesized Bi_2Te_3 nanotubes of 100 nm diameter and 500–1000 nm length via hydrothermal route using sodium borohydride as a reductant and EDTA as surfactant however they have carried out this experiment in beaker rather than a steel autoclave [54]. Although working with autoclave in an electric furnace may be safe but hydrothermal reactions may be carried out in glassware as well.

2.2. Solvothermal method

In chemistry, effect of reaction conditions and environment is very important. If we replace water in hydrothermal method then the process will be called as solvothermal. Keeping aside the curiosity of using other solvent/s instead of water there are sometimes problems of oxide and hydroxide formation with certain metals. Water is strongly hydrogen bonding solvent and lone pair on its oxygen is easily donatable to form labile coordination complexes with transition metals. While using water,

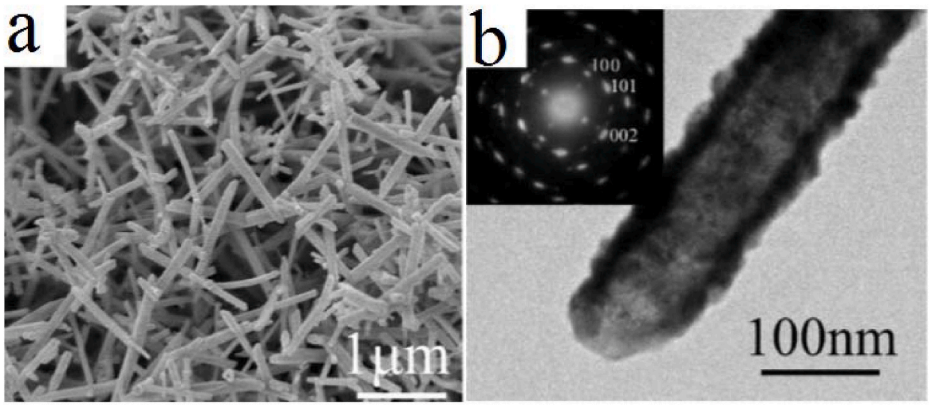

Fig. 2. FESEM and HRTEM images of CoTe nanotubes. Modified from Refs. [49]. Copyright ACS 2008.

we cannot achieve a reaction temperature of more than 100 °C.

$CoTe_2$ nanotubes have been fabricated by using a mixture of ethylene glycol and OA (5:3) as solvents under solvothermal conditions (Table 1) [55]. Time dependent studies show that Te is converted to hexagonal Te nanotubes after 3 h of experiment (Fig. 3) and serve as in situ templates. After 3 h, conversion of Te nanotubes to $CoTe_2$ nanocrystals starts and after 5 h their peaks are evident in PXRD. After 5 h smooth surface of Te nanotubes becomes rough with emergence of small $CoTe_2$ nanoparticles (Fig. 3f). After 12 h the product is predominantly $CoTe_2$ but with the impurities of hexagonal Te. After 24 h of reaction pure $CoTe_2$ nanotubes were obtained [55]. Self sacrificing of Te templates and alloying process was proposed to be the mechanism of this reaction. During self sacrifice, freshly prepared Te nanotubes of high chemical activities react with metal to form telluride nanoparticles. During alloying process, cobalt atoms produced by reduction with ethylene glycol diffuse in Te nanotubes to form $CoTe_2$ nanoparticles on the surface of Te nanotubes. This growth process in one dimensional confined space produced $CoTe_2$ nanotubes. This method was further extended for the synthesis of CdTe, PbTe, Sb_2Te_3 and Bi_2Te_3.

First attempt on In_2Te_3 nanotubes of 500 nm diameter and 50–100 nm thickness at different reaction temperatures, reaction times, PVP and ethylene diamine addition was made with solvothermal method [56]. At lower temperature (100–120 °C) nanorods are formed and nanotubes are only formed above 160 °C. After 12 h of reaction, mostly nanowires are obtained and predominant formation of nanotubes is achieved after 48 h only. As for as PVP is concerned, its addition definitely plays a role during alignment of species and its optimal concentration used in this study was 1140 mg. Further studies are still required to have a clear picture about the role of PVP. Higher is the concentration of ethylene diamine, formation of nanoparticles instead of nanotubes is favored. Nucleation of In_2Te_3 nanotubes starts by the reduction of TeO_3^{2-} to Te or Te^{2-}. Then on the circumferential edges of these reduced species, next growth starts on c-direction. This preferential growth on one direction may have yielded final nanotubular product. Covalent bonded growth along c-axis is faster which gives length to the tubes than the van der Waals interactions which provide thickness along circumference [56].

2.3. Electrodeposition

Electrodeposition is the oldest method for the fabrication of nanomaterials via templates. Template pores can be filled with electroless deposition, sol gel method, chemical vapor deposition and physical vapor deposition etc. but electrodeposition is the most reliable technique for nanowires and nanorods. Two important factors for smooth deposition are applied potential and deposition rate (diffusion of ions to the deposition site). For fracture free smooth growth an additional amount of overpotential is also important to consider.

Bismuth telluride nanotubes have been deposited using PC (poly carbonate) sputtered with gold as working electrode and saturated calomel (SC) as reference electrode [57]. Electrolyte consisted of 0.01 M bismuth oxide and 0.01 M tellurium oxide in 2 M nitric acid. PC template produced nanotubes with an outer and inner diameter of 360 ± 15 nm and 240 ± 12 nm respectively at −400 mV. At −65 mV vs. SCE outer and inner diameter of nanotubes were 310 ± 10 nm and 210 ± 15 nm respectively [57]. Wall thickness of nanotubes at −400 mV and −65 mV were ~60 ± 3 and ~50 ± 5 nm respectively. Fabrication at higher potential yielded p-type (Bi rich) and at lower potential produced n-type (Te rich) bismuth telluride. Formation of nanotubes instead of nanowires is because of gold which is present at the bottom wall of PC templates and it promotes deposition in this region. Consequent gas

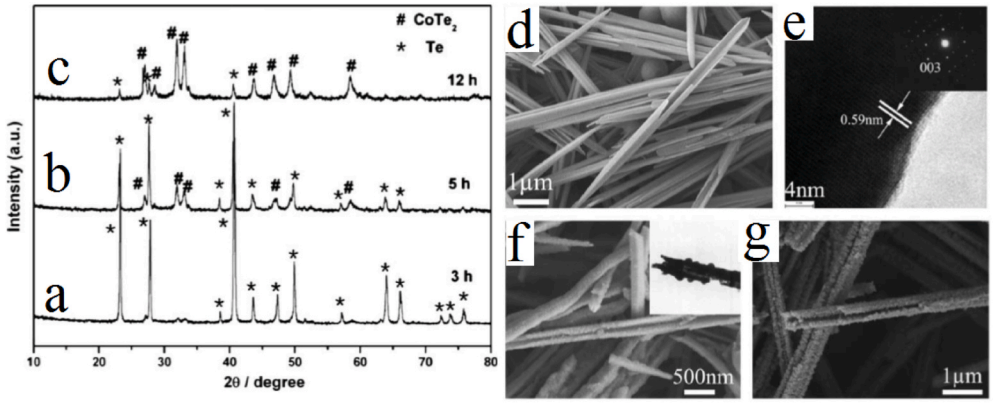

Fig. 3. PXRD patterns after a) 3 h, b) 5 h, c) 12 h, d) SEM image Te nanotubes after 3 h, e) HRTEM of Te nanotubes, f) SEM and TEM (inset) of product after 5 h, g) SEM image of product after 12 h. Reproduced with permission from Refs. [55]. Copyright Elsevier 2009.

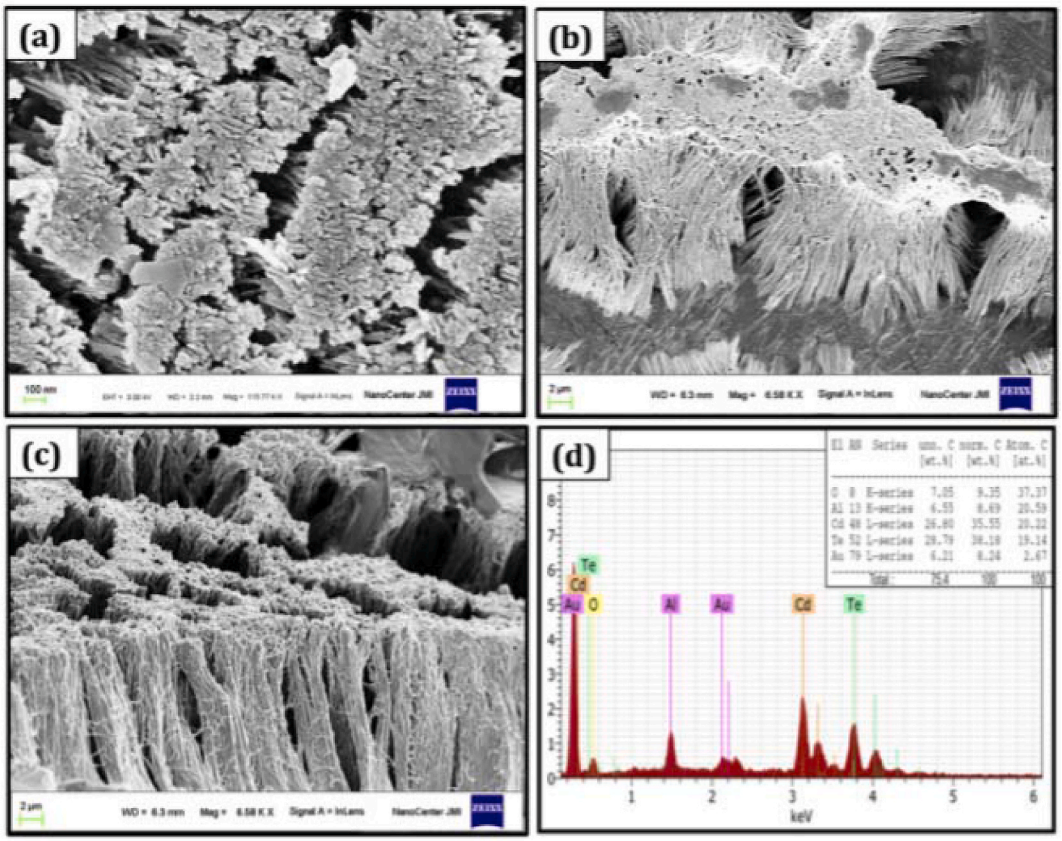

Fig. 4. FESEM micrographs of CdTe nanotubes a) top view, b) side view, c) cross sectional view, d) EDX of CdTe nanotubes. Reproduced with permission from Ref. [58]. Copyright Elsevier 2019.

evolution during deposition process may have restricted the growth in centre region of pores to favor nanotubular morphology [57].

Electrodeposition has been used to fabricate CdTe nanotubes on anodic aluminum oxide (AAO) as template and working electrode, Pt mesh as a counter electrode and Ag/AgCl as a reference electrode. Electrolyte composition was 0.05 M cadmium sulfate, 0.005 M tellurium oxide in 1 M sulfuric acid in sulfate bath and 0.05 M cadmium chloride with 0.005 M tellurium oxide in 1 M hydrochloric acid in chloride bath at pH 2 which was maintained by dropwise addition of sodium hydroxide. Deposition was carried out at 598 mV with 0.02–0.13 mA (DC) for 1 h at 70 °C. At completion of deposition AAO was dissolved in 2 M sodium hydroxide for 30 min at 50 °C. During cathodic polarization in sulfuric acid, protons are dissociated from electrolyte and are reduced to molecular hydrogen at AAO [58]. Hydroxide is produced at pore bottom and decomposes the barrier layer with increase in pH. Reactions at cathode are as under [58];

$$2H^+ + 2e^- \rightarrow H_{2(g)} \quad (1)$$

$$2OH^- + Al_2O_3 \rightarrow 2AlO_2^- + H_2O \quad (2)$$

$$AlO_2^- + H_2O + H^+ \rightarrow Al(OH)_3 \quad (3)$$

Reaction at anode is

$$4OH^- \rightarrow 2H_2O + O_2 + 4e^- \quad (4)$$

In sulfate bath well aligned arrays of CdTe nanotubes (80 ± 10 nm diameter) were produced (Fig. 4). Whereas in chloride bath 3D superstructure microflower composed of Te rich nanorods are produced. Electrochemical reactions for this experimental fact are as under;

$$HTeO_2^+ + 3H^+ + 4e^- \rightarrow Te_{(s)} + 2H_2O \; E = 0.55 \text{ V vs. NHE} \quad (5)$$

$$Cd^{2+} + 2e^- \rightarrow Cd_{(s)} \; E = -0.4 \text{ V vs. NHE} \quad (6)$$

$$Cd^{2+} + Te_{(s)} + 2e^- \rightarrow CdTe_{(s)} \; E = 0.55 \text{ vs. NHE} \quad (7)$$

Chloride ions in comparison to sulfate ions change the deposition of CdTe by suppressing the activity of $HTeO_2^+$. This shifts the equilibrium curve of $HTeO_2^+/Te^-$ to less positive potential and hinders the formation of CdTe [58].

In another attempt nickel nanotubes were synthesized by electroless deposition and were used as a sacrificial template for the fabrication of bismuth telluride nanotubes (outer diameter 634 ± 16 nm and wall thickness 52 ± 2 nm) via galvanic displacement reaction [59]. During galvanic displacement reaction elemental nickel reduces bismuth and tellurium ions according to following equation;

$$2Bi^{3+}{}_{(aq)} + 3HTeO_2^+{}_{(aq)} + 9Ni_{(s)} + 9H^+{}_{(aq)} \rightarrow Bi_2Te_{3(s)} + 9Ni^{2+}{}_{(aq)} + 6H_2O_{(aq)} \quad (8)$$

2.4. Chemical synthesis

Chemical methods for the synthesis of nanomaterials are conventional, comparatively mild and are carried out in glassware. Use of immiscible solvent interface for the synthesis of nanoparticles is well reported but self assembly of these nanoparticles to hollow spheres and then to nanotubes has been reported for CdTe [60]. In a typical synthesis CdTe quantum dots (QDs) were prepared by the reaction of Cd^{2+} and NaHTe in the presence of thioglycolic acid (TGA) as a surfactant. $\sim 10^{-3}$ M aqueous solution of these CdTe QDs was mixed with acetone (35 mL) and dodecanthiol (10 mL) in a 100 mL round bottom flask. Reaction mixture was refluxed with vigorous magnetic stirring. Mixing of QDs to DDT took minutes for the formation of nanoparticles which were

transformed to nanotubes after 4 h of reaction [60]. Surface of CdTe is passivated with TGA in aqueous phase. When CdTe QDs are transferred to DDT, there is extraction of QDs to DDT (the nonpolar solvent). According to authors, this extraction process is not much efficient due to small interface between water and DDT. When acetone is added in the reaction mixture which is miscible with both water and DDT, this interface is converted to an emulsion. In this emulsion CdTe nanoparticles get the privilege of interaction with two ligands i.e. TGA and DDT. TGA is attached on the surface of CdTe nanoparticles with thiol functionality in aqueous phase whereas carbonyl is free to bind with other species. When CdTe nanoparticles are transferred from aqueous phase to organic phase there is a competition between TGA and DDT for binding. The interaction between TGA and DDT forms the basis for hollow spheres which are then converted to hollow nanocylinders and finally to CdTe nanotubes (Fig. 5).

Another chemical strategy for the synthesis of Bi_2Te_3 nanotubes is the reaction of Bi precursor (Bi-TOPO) with Te precursor (Te-TOPO) in a way that Te nanowires serve as a template [61]. For the synthesis of Te nanowires Te-TOPO is swiftly injected in a hot solution (200 °C) of OA and OlA. After the synthesis of Te nanowires, temperature of flask is reduced to 80 °C and Bi-TOPO precursor and phenyl hydrazine are simultaneously injected in it. Exothermic reaction increases the temperature to 86 °C but 80 °C is maintained after 5 min. Reaction is carried out for 12 h at this temperature for completion and then winding up steps of washing give Bi_2Te_3 nanotubes. Lower temperature (80 °C) is mandatory for uniform growth of nanotubes because if the reaction s carried out at higher temperature, enough time is not available for smooth growth of nanotubes. Bi nanoparticles are produced from Bi-TOPO and get attached on the surface of Te nanowires. Under the experimental conditions, Bi and Te layers diffuse mutually in an alloying process to form Bi_2Te_3. Outward diffusion of Te from nanowires especially at high diffusivity may be a reason for nanotubes formation. If all the reactants above are mixed together and reaction is carried out hydrothermally, Bi_2Te_3 nanotubes can be generated but they are of poor quality. Drawback with chemical synthetic methods is that they depend on too much variables such as type of reactants and their mixing sequence, reaction temperatures, reaction times, type of reductants and their concentrations [62], type of capping agents and their concentrations which make these methods industrially unfavorable. Moreover people who work on the application of synthesized nanomaterials have no expertise in such type of difficult methodologies. They favor simple methods of synthesis for practical applications concerns [61].

2.5. Microwave methods

A microwave synthetic method is advantageous in terms of higher reaction rates, rapid volumetric heating, better selectivity and shorter reaction time. Bi_2Te_3 hollow nanospheres have been reported by this method [63] but first successful attempt of Bi_2Te_3 nanotubes was put forth by Qin Yao et al. [64]. In this methods bismuth nitrate solution was prepared in a flask using ethylene glycol as a solvent and heated at 170–195 °C by microwave (2.45 GHz). In this flask, second solution of TeO_2 in nitric acid and ethylene glycol was added. The mixture was maintained as such for 30–60 min to get Bi_2Te_3 nanotubes which were washed with 1 M nitric acid after centrifugation [64]. In this method, nanosheets are formed at 180 °C, nanosheets with folding were observed at 190 °C and majority of nanotubes were observed at 195 °C (Fig. 6). Above 180 °C, reducing ability of ethylene glycol may convert metal ions to zero oxidation state according to the equations below;

$$3HTeO_2^+ + 9H^+ + 4e^- \rightarrow 3Te + 6H_2O \; E = 0.56 \text{ V} \quad (9)$$

$$2Bi^{3+} + 6e^- + 3Te \rightarrow Bi_2Te_3 \; E = 0.45 \text{ V} \quad (10)$$

Over all reaction will be written as

$$3HTeO_2^+ + 2Bi^{3+} + 9H^+ + 18e^- \rightarrow Bi_2Te_3 + 6H_2O \quad (11)$$

Due to higher reduction potential of Eq (9) than Eq (10), higher concentrations of Te will be available for lower concentrations of Bi^{3+}. Therefore comparatively higher concentration of Bi^{3+} is necessary at the start of reaction to move forward (10) and to avoid Te impurity in the final product [64].

2.6. Combination processes

Sometimes combination of different processes is required to

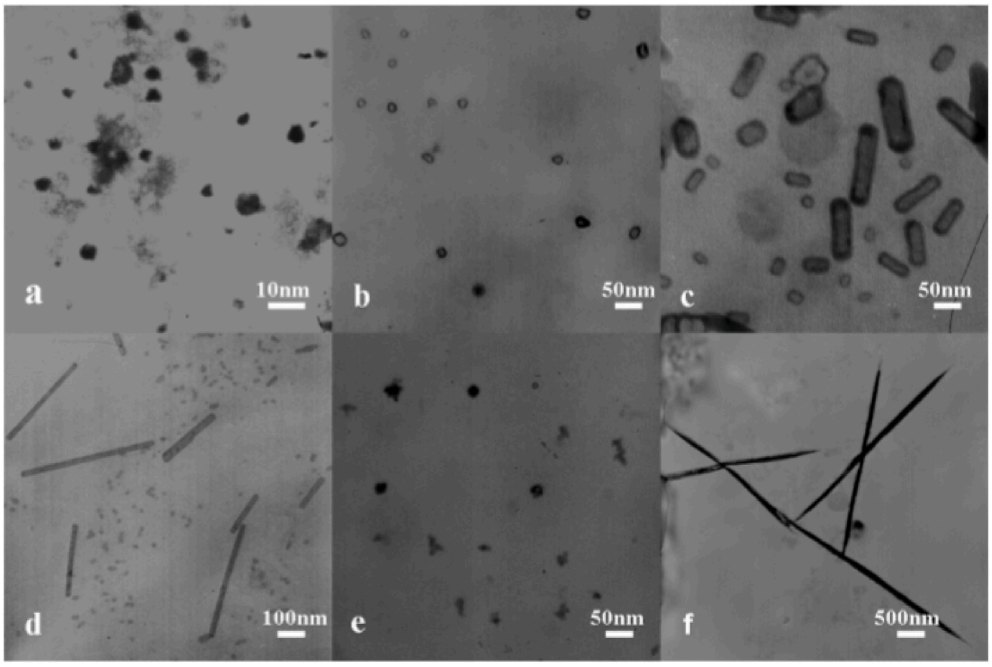

Fig. 5. TEM images of CdTe a) nanoparticles after several minutes, b) hollow nanospheres after 1 h, c) hollow nanocylinders after 2 h, d) nanotubes after 4 h, e) fragments after 5 h, f) nanowires after 6 h. Reproduced with permission from Refs. [60]. Copyright Royal Society of Chemistry 2009.

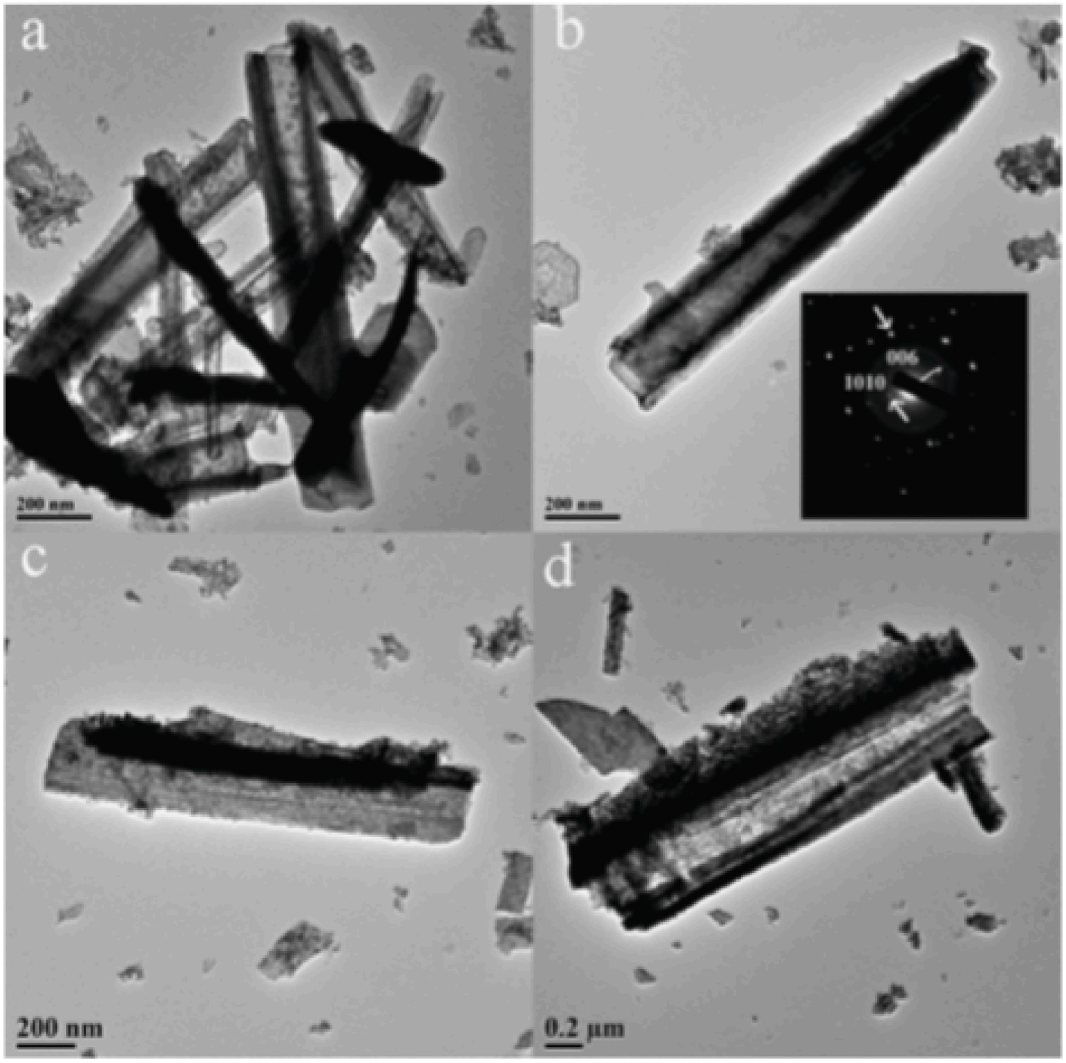

Fig. 6. TEM images of Bi_2Te_3 at 195 °C for 30min (a and b) nanotubes, inset of (b) ED pattern of nanotubes, (c and d) TEM images of the nanosheet bending in width direction. Reproduced with permission from Refs. [64]. Copyright Elsevier 2009.

synthesize the desired nanotubes. CdTe [65] and PbTe [66] nanotubes have been synthesized by combination of electrospinning, electrodeposition and cation exchange reaction. CdTe nanotubes have wall thickness (7 nm) and length (22 nm) in nanometer range when synthesized with conventional water oil (dodecanethiol) interface method [60]. By using positives of different methods, desired CdTe nanotubes are achieved comparatively easily. For CdTe nanotubes, first Ag nanofibers were produced by mixing PVP and silver nitrate in water/ethanol and homogenizing them for 12 h. This solution was then fed with capillary tube (0.14 mm diameter) at a fixed flow rate of 0.2 mL/h in a drum collector on a glass substrate at 20 KV. This produced electrospun $AgNO_3$/PVP fiber which were reduced to Ag nanofibers by calcinations in hydrogen at 150 °C for 3 h and then at 250 °C for 90 min at 2 °C/min. These silver wires were electrotellurated with 10 mM $HTeO_2^+$ solution in 1 M nitric acid using Ag/AgCl as a reference and Pt as a counter electrode. As prepared Ag_2Te nanotubes [67] on glass substrate were immersed in 50 mM cadmium nitrate solution using 20 mL of methanol. Cation exchange produced ultra long zinc blende CdTe nanotubes with controlled dimensions and morphology (Fig. 7). Transformation of silver telluride to cadmium telluride is not thermodynamically favorable due to lower Ksp value of silver telluride. This process is made kinetically favorable by the addition of TBP which forms complex with silver ions to shift the balance of reaction towards cadmium telluride.

Antimony telluride nanotubes have been fabricated by combining microwave assisted heating of solvothermal mixture in a Teflon autoclave via template free process [68]. Advantage of microwave heating for solvothermal process is the requirement of minimal time (15 min) as compared to hours in furnace heating [68]. Chemical reactions involved in this process are as under;

$$TeO_2 + N_2H_4 \rightarrow Te + N_2 + 2H_2O \quad (12)$$

$$2Te + N_2H_4 + 4OH^- \rightarrow 2Te^{2-} + N_2 + 4H_2O \quad (13)$$

$$2Sb^{3+} + 3Te^{2-} \rightarrow Sb_2Te_3 \quad (14)$$

Another combination approach is the synthesis of bimetallic $Ni_{0.33}Co_{0.67}Te$/Ni composites via solvothermal process first and then their conversion to nanotubes during ion exchange [69]. Use of hydrazine in solvothermal reaction is important because it reduces the tellurium precursor via following reaction;

$$3N_2H_4 + 2TeO_3^{2-} \rightarrow 2Te^{2-} + 6H_2O + 3N_2 \quad (15)$$

Ion exchange is between hydroxyl and nitrate ions of $(Ni_{0.33}Co_{0.67})_3(NO_3)_2(OH)_4$ and Te^{2-} ions which are produced during reaction (15). During ion exchange, conversion of nanosheets to nanotubes starts after 10 h and is completed after 12 h. Length of these nanotubes is 10 μm and diameter is ~40 nm. These reaction timings are necessary to be followed strictly because when reaction time reaches 15

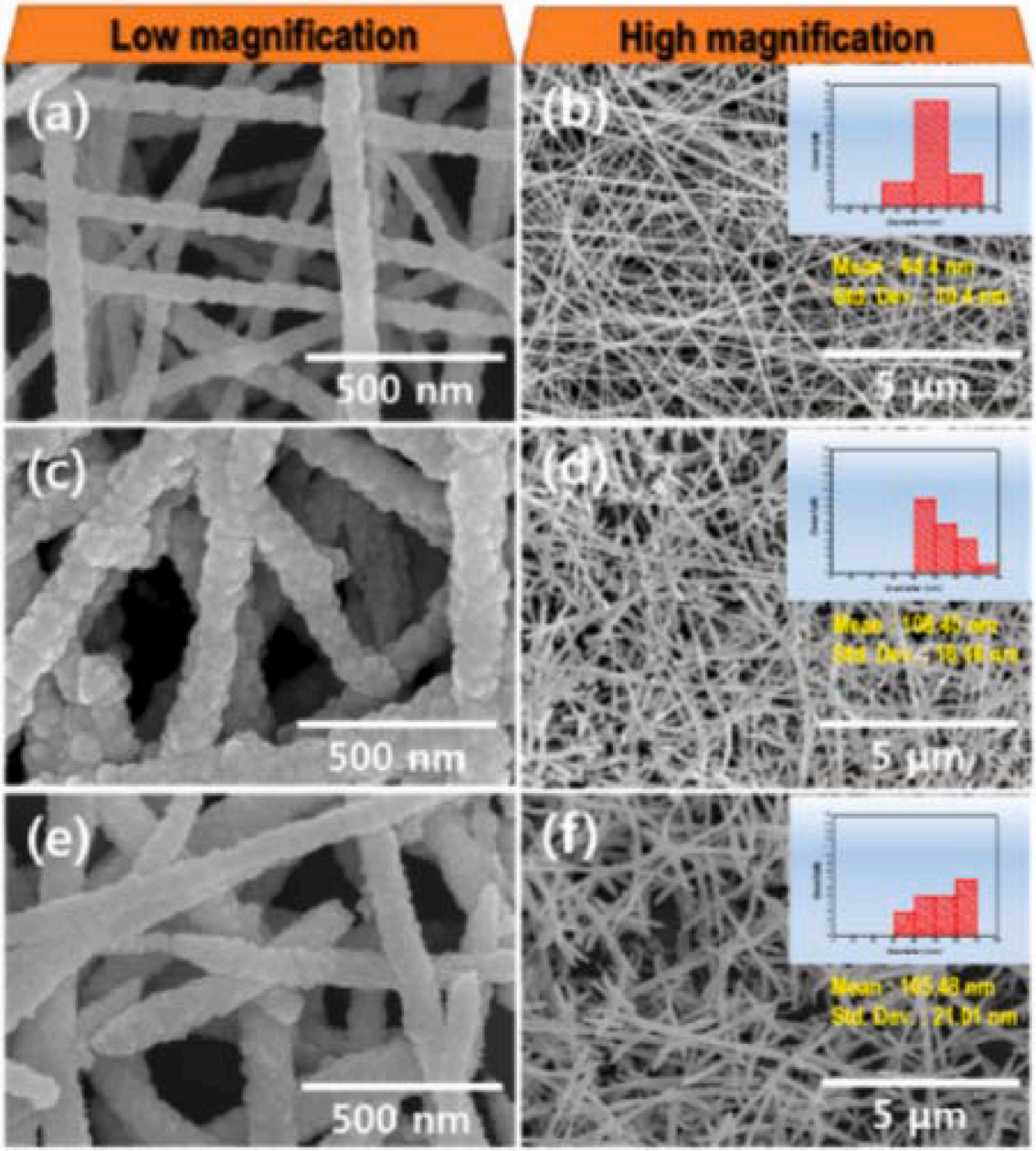

Fig. 7. SEM micrographs of (a, b) Ag nanofibers, (c, d) Ag_2Te nanotubes and (e, f) CdTe nanotubes. Reprinted with permission from Refs. [65]. Copyright Elsevier 2017.

h, internal diameter of nanotubes increases and some tubes show deformation as well. If concentrations of reactants are not proper say for example at higher concentrations of Na_2TeO_3 linear tubular structure is converted to thick aggregates of sheets. Retention of nanotubular structure synthesized at 180 °C after 12 h is necessary for optimal electrochemical performance [69].

3. Applications of metal telluride nanotubes

3.1. Thermoelectric applications

Thermoelectric materials are important because they covert thermal power to electrical power by Seebeck effect. This electrical power is generated by temperature difference. Another important effect is the Peltier effect which makes use of electrical energy for refrigeration. Both these effects have not achieved industrial excellence because of poor conversion efficiencies of thermoelectric materials relative to mechanical systems requirements. Efficiency of a thermoelectric material is measured by a dimensionless figure of merit $ZT = S^2\sigma T/k$, where T is the absolute temperature, σ is electrical conductivity, S is the Seebeck coefficient and k is the thermal conductivity. In a semiconducting material all these parameters are mutually interdependent and best thermoelectric materials manufactured so far have a $ZT = \sim 1$. If scientists are able to improve the efficiency of thermoelectric materials then problem of noise, working fluid and moving part aging and failure associated with conventional coolers and power generators can be tackled.

Different morphologies of antimony telluride were investigated for their thermoelectric properties [68]. Antimony telluride nanorods with branched nanosheets have S values of 275–332 μV/K which are better than half nanotubes (214–257 μV/K). S value of antimony telluride nanosheets (194–245 μV/K) are superior than antimony telluride nanorods (166–211 μV/K) [68]. This difference in S values may be

attributed to size effects and self assembly of antimony telluride. However in this study, clear cut demarcation between antimony morphologies was not available i.e. there were mixtures of different shapes.

Nanotubular hot pressed Bi_2Te_3 and PbTe samples have inferior S values as compared to melt samples (Fig. 8). This may be attributed to the hindrance caused by the grain boundaries in the flow of electrons. Similarly, thermal conductivities of nanotubular hot pressed Bi_2Te_3 and PbTe samples are approximately 80% lower than the melt samples. This may be due to the scattering of phonons on grain boundaries owing to polycrystalline nature of samples [61,70]. This suppression of thermal conductivity of Bi_2Te_3 nanotubes (0.62 W/mK at 470 K) has also been reported by other workers [71]. However maintenance of high electrical conductivity in this study was attributed to high crystalline nature of Bi_2Te_3 nanotubes which gave a power factor of 9.08–10.3 μW/cmK^2 and ZT value of 0.77 at 464 K [71]. Performance of Bi_2Te_3 can be improved by incorporating the impurity of potassium to synthesize $K_{0.06}Bi_2Te_{3.18}$ [72]. This incorporation increases the power factor to ~43 μW/cmK^2 with a high ZT value of >1.1 at 323 K. This high power factor is due to unconventional electron donation by potassium ions [72]. Thermal conductivities of Bi_2Te_3 nanotubes are lower than nanowires due to additional scattering of electrons at side walls of nanotubes. This gives almost double ZT values to nanotubes than nanowires [73].

3.2. Electrochemical water oxidation

Due to increase in population of mankind on our planet, pollution free energy demand has increased. Among many other environmental friendly technologies (fuel cells, solar cells, batteries, supercapacitors etc.), water splitting is an important domain to aim at. Catalysts which have given acceptable performances for water splitting are noble (Pt, Ir, Ru) metal oxides and are rare in earth crust [74–77]. These limitations make them industrially rejected. So, this is need of the time to have a catalyst of relatively abundant and less precious metals or their compounds for water oxidation. Extensive research has been carried out in this regard using transition metal oxides, sulfides and selenides [2–4, 78–81]. CoTe nanotubes deposited on FTO glass from aqueous solutions, have been evaluated for hydrogen and oxygen evolution reactions (OER) [50]. Overpotential for oxygen evolution reaction is 0.37 V (without iR compensation) at 10 mA/cm^2. This performance is attributed to enhanced electrochemical surface area and improved electrical conductivity via intergranular connectivity [50]. This OER performance of CoTe films annealed at 200 °C is comparable to state of the art Ir catalyst (0.35 V at 10 mA/cm^2) [82] and is better than other chalcogenides reported in literature such as $CoTe_2$ (0.357 V) [83], CoTe (0.365 V) [83], $CoTe_2/CoO_x$ (0.38 V) [84], $NiCo_2S_4$@N/S-rGO (0.47 V) [85] and Co_9S_8@MoS_2/C NFs (0.43 V) [86].

3.3. Supercapacitive applications

Portable electronic devices are the requirement in modern era. These devices require portable energy storages of high energy density and high power density. Supercapacitors are energy storage devices which have high power density, high energy density, long cycle stability, swift charge discharge and are secure as well. But there is a drawback when we compare supercapacitors with commercial batteries in terms of lower energy densities. Recently different hybrid materials of Co and Ni have been evaluated for their supercapacitive behavior [87–89]. In this realm nanotubes of $Ni_{0.33}Co_{0.67}Te$ on Ni foam have been recently evaluated for supercapacitive behavior [69]. In a three electrode system, $Ni_{0.33}Co_{0.67}Te$ on Ni foam was used as free standing working electrode, Hg/HgO as a reference and Pt foil as a counter electrode. In cyclic voltammetry (CV) scan rates were between 5 and 200 mV/s and in galvanic charge discharge (GCD) current densities were between 1 and 20 A/g. Fig. 9a presents the nonlinear GCD of $Ni_{0.33}Co_{0.67}Te$ nanotubes. High specific capacity of $Ni_{0.33}Co_{0.67}Te$ nanotubes is due to high specific surface area and excellent contact between electrode and electrolyte. Oxidation and reduction maxima in CV profile (Fig. 9c) at different scan rate confirm the faradaic reactions during energy storage process. Fig. 9b presents the specific capacities of optimized $Ni_{0.33}Co_{0.67}Te$ nanotube electrode which are 131.2, 116.2, 108.4, 99.3, 89.1, 83.6 and 79.3 mA h/g at current densities of 1, 2, 3, 5, 10, 15 and 20 A/g, respectively. $Ni_{0.33}Co_{0.67}Te$ nanotube electrode show long cycle stability at 5 A/g i.e. 92% after 5000 cycles (Fig. 9e). This excellent performance owe to; i) efficient electron transfer and diffusion in the porous hierarchical $Ni_{0.33}Co_{0.67}Te$ nanotubes, ii) non aggregation caused by hindrance of volume changes during electrochemical reactions by interpenetrating network of nanotubes and iii) rich redox reaction of bimetallic electrode due to its high electrical conductivity (3.30×10^4 m/S). Furthermore $Ni_{0.33}Co_{0.67}Te$/AC (activated carbon) hybrid supercapacitor shows energy density of 54 W h/Kg and power density of 918 W/kg at an operating voltage of 1.6 V. This energy density is maintained at 31.9 W h/Kg which is better than $Ni_{0.67}Co_{0.33}Se$/RGO (36.7 W h/kg at 750 W/kg) [90], H–$NiCoSe_2$/AC (25.5 W h/kg at 3750 W/kg) [91], $Ni_{0.5}Co_{0.5}Se_2$//RGO (37.5 W h/kg at 750 W/kg) [92], $Ni_{0.33}Co_{0.67}/Se_2$/AC (29.1 W h/kg at 800 W/kg) [93], NiTe:Co/AC (36.8 W h/kg at 800 W/kg) [89] and CoTe/AC (23.5 W h/kg at 793.5 W/kg) [94].

4. Conclusions and future horizons

Metal tellurides nanotubes can be synthesized with and without templates. Templated synthesis of metal telluride is identical to all other binary inorganic materials but nontemplated synthesis of metal telluride nanotubes is due to their inherent structural bending just like their sulfur and selenium analogues. Length and internal diameter of metal telluride nanotubes synthesized via hydrothermal/solvothermal methods

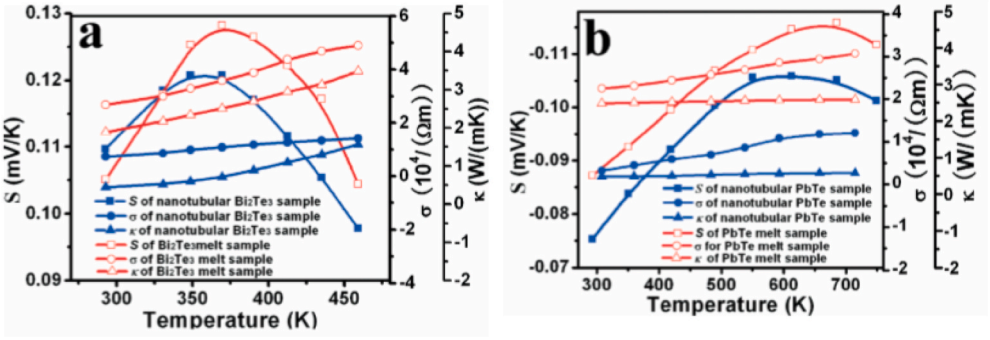

Fig. 8. Comparative thermoelectric properties of hot-pressed nanotubular and melted Bi_2Te_3 and PbTe. Reproduced with permission from Ref. [70]. Copyright Royal Society of Chemistry 2014.

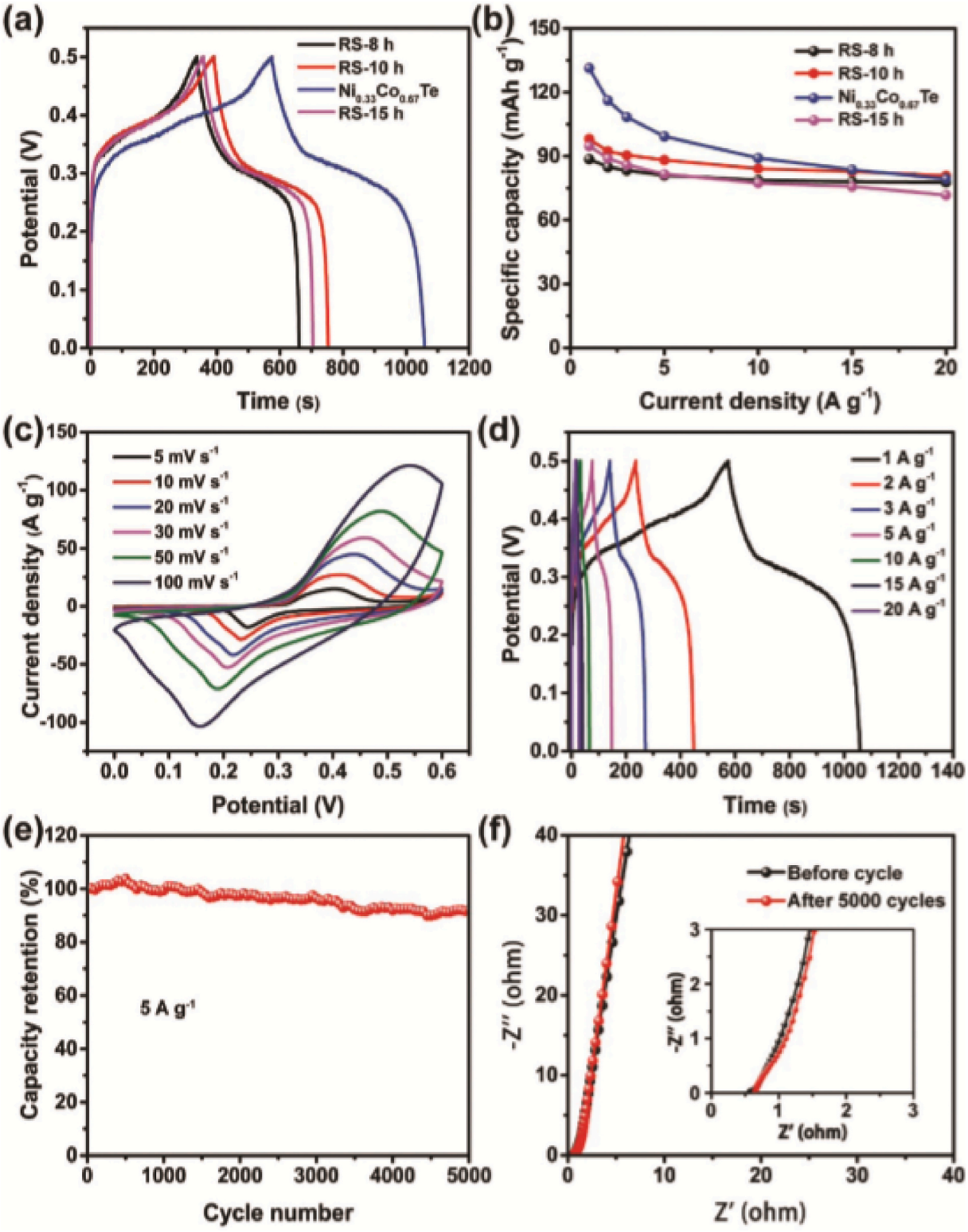

Fig. 9. a) Galvanic charge discharge curves, b) specific capacities of the as-prepared electrodes with different reaction times c) cyclic voltammetry curves, d) galvanic charge discharge curves, (e) cycling stabilities at 5 A/g, f) Electronic impedance spectroscopic spectra before and after 5000 cycles of the optimized $Ni_{0.33}Co_{0.67}Te$/Ni foam electrode. Reprinted with permission from Ref. [69]. Copyright Royal Society of Chemistry 2020.

depends upon concentration of capping agent (ammonia, glucose, EDTA, etc.), reaction time and reaction temperature. Generally higher reaction times and higher reaction temperatures are recommended for nanotubes to grow but conditions have to be optimized for particular types and dimensions of nanotubes.

In electrodeposition polycarbonate, anodic aluminum oxide and nickel nanotubes have been used as templates for synthesis of bismuth telluride, cadmium telluride and bismuth telluride, nanotubes, respectively. Compositions of bath, deposition potentials and pH have to be optimized for telluride nanotubes of specific internal diameter and

lengths.

Chemical methods for synthesis of metal telluride nanotubes are complex combination of a sequence in which type of reactants, their mixing sequence, their concentrations, time of reaction, capping agents and reductants are very important. Templates are generally produced in situ and a main difference with hydrothermal methods is that nanotubular morphology is favored at comparatively lower temperatures in chemical methods. Microwave method is advantageous due to higher rate of reactions and this method also supports higher temperature hypothesis for nanotubes formation.

Metal tellurides of bismuth, copper, mercury, antimony, nickel, lead, zinc, cobalt, cadmium, indium and molybdenum have been reported in literature. Some of these materials were converted to nanotubes which was the focus of this review however there remains a thirst in this field for the synthesis of other transition metal tellurides. One problem is common for all the methods discussed above for the synthesis of metal tellurides i.e. more affinity of metals with oxygen than tellurium. To tackle this problem different strategies are followed in different methods. In hydro/solvothermal methods reductants are used. To optimize the concentration of reductants is the main task for synthetic chemists. In case of electrochemical methods especially cyclic voltammetry, cells containing the electrolytic media have to be purged with inert gases (nitrogen or argon). Chemical methods require the use of vacuum lines or glove boxes to avoid the contamination of oxide phase/s in the telluride products. Except electrodeposition all other methods produce metal tellurides with surface defects which are however favorable for different device application. When we discuss nanotubular morphology of metal tellurides, methods such as chemical vapor deposition, chemical vapor transport, spin coating, laser beam epitaxial growth, aerosol assisted chemical vapor deposition, solid state reactions, chemical bath deposition, sol gel method, sputtering methods etc. are not common. Applications of metal telluride nanotubes have not been investigated in detail. Applications studies are at the level of nanoscience only and much more remain to achieve nonotechnologically. To the best of our knowledge no product of metal telluride nanotubes has been marketed yet.

Declaration of competing interest

The authors declare that they have no known competing financial interests or personal relationships that could have appeared to influence the work reported in this paper.

Acknowledgements

This work has no financial support or funding from any organization.

References

[1] R.A. Hussain, A. Badshah, B. Lal, Fabrication, characterization and applications of iron selenide, J. Solid State Chem. 243 (2016) 179–189.
[2] R.A. Hussain, I. Hussain, Fabrication and applications of nickel selenide, J. Solid State Chem. 277 (2019) 316–328.
[3] R.A. Hussain, I. Hussain, Copper selenide thin films from growth to applications, Solid State Sci. 100 (2020) 106101.
[4] R.A. Hussain, I. Hussain, Cadmium selenide nanowires from growth to applications, Mater. Res. Express 6 (2020) 122007.
[5] U. Shamraiz, R.A. Hussain, A. Badshah, Fabrication and applications of copper sulfide (CuS) nanostructures, J. Solid State Chem. 238 (2016) 25–40.
[6] Um-e-Habiba, A. Badshah, R.A. Hussain, Synthesis of iron chalcogenides from single source precursors, Appl. Organomet. Chem. 30 (2016) 783–795.
[7] R. Chianelli, E. Prestridge, T. Pecoraro, J. DeNeufville, Molybdenum disulfide in the poorly crystalline “Rag” structure, Science 203 (1979) 1105–1107.
[8] S. Iijima, Helical microtubules of graphitic carbon, Nature 354 (1991) 56–58.
[9] C.N.R. Rao, M. Nath, Inorganic nanotubes, advances in chemistry: a selection of CNR Rao’s publications (1994–2003), World Sci. (2003) 310–333.
[10] R. Tenne, L. Margulis, M.e. Genut, G. Hodes, Polyhedral and cylindrical structures of tungsten disulphide, Nature 360 (1992) 444–446.
[11] M. Steigerwald, T. Siegrist, S. Stuczynski, Initial stages in the molecule-based growth of the solid-state compound cobalt telluride (CoTe), Inorg. Chem. 30 (1991) 4940–4945.
[12] B. Wang, M. Zhu, H. Wang, G. Dong, Study on growth and photoluminescence of zinc telluride crystals synthesized by hydrothermal method, Opt. Mater. 34 (2011) 42–47.
[13] V. Kloper, R. Osovsky, J. Kolny-Olesiak, A. Sashchiuk, E. Lifshitz, The growth of colloidal cadmium telluride nanocrystal quantum dots in the presence of Cd0 nanoparticles, J. Phys. Chem. C 111 (2007) 10336–10341.
[14] Z.M. Alvand, H.R. Rajabi, A. Mirzaei, A. Masoumiasl, Ultrasonic and microwave assisted extraction as rapid and efficient techniques for plant mediated synthesis of quantum dots: green synthesis, characterization of zinc telluride and comparison study of some biological activities, New J. Chem. 43 (2019) 15126–15138.
[15] V. Smetana, M. Wilk-Kozubek, A.-V. Mudring, Active-transition-metal tellurides: through crystal structures to physical properties, Cryst. Growth Des. 19 (2019) 5429–5440.
[16] W. Hönle, H. Von Schnering, A. Lipka, K. Yvon, New compounds with infinite chains of face-condensed octahedral Mo6 clusters: InMo3Se3, InMo3Te3, TlMo3Se3 and TlMo3Te3, J. Less Common. Met. 71 (1980) 135–145.
[17] H. Ma, P. Chen, B. Li, J. Li, R. Ai, Z. Zhang, G. Sun, K. Yao, Z. Lin, B. Zhao, Thickness-tunable synthesis of ultrathin type-II Dirac semimetal PtTe2 single crystals and their thickness-dependent electronic properties, Nano Lett. 18 (2018) 3523–3529.
[18] A. Kolb, KurtO. Klepp, K4Ti3Te9–A new pseudo one-dimensional polyanionic alkali chalcogenometallate (IV), Z. Naturforsch. B Chem. Sci. 58 (2003) 633–638.
[19] K.O. Klepp, A. Kolb, Komplexe Chalkogenide der IVa Metalle mit niedrigdimensionalen anionischen Partialstrukturen. Darstellung und Kristallstruktur von K2ZrTe3 und Rb2ZrTe3/Complex Chalcogenides of the IVa Metals with Low Dimensional Anionic Partial Structures. Preparation and Crystal Structures of K2ZrTe3 and Rb2ZrTe3, Z. Naturforsch. B Chem. Sci.: J. Chem. Sci. 54 (1999) 441–446.
[20] P. Villars, K. Cenzual, J. Daams, R. Gladyshevskii, O. Shcherban, V. Dubenskyy, N. Melnichenko-Koblyuk, O. Pavlyuk, S. Stoiko, L. Sysa, CsTaTe3, Structure Types. Part 3: Space Groups (194) P63/mmc-(190) P-62c, Springer, pp. 1-1 .
[21] P. Matje, W. Müller, H. Schäfer, Zur Darstellung und Kristallstruktur von Ba2MnTe3/Preparation and Crystal Structure of Ba2MnTe3, Z. Naturforsch. B Chem. Sci. 32 (1977) 835–836.
[22] Y. Wang, F. DiSalvo, Synthesis and structural characterization of Ba2CdTe3, J. Solid State Chem. 148 (1999) 464–467.
[23] M.-J. Li, C.-L. Hu, X.-W. Lei, Y. Zhou, J.-G. Mao, Syntheses, crystal and electronic structures of three new potassium cadmium (II)/zinc (II) tellurides: K2Cd2Te3, K6CdTe4 and K2ZnTe2, J. Solid State Chem. 182 (2009) 1245–1251.
[24] S. Dehnen, S. Burtzlaff, M. Holynska, Synthesis and crystal structures of K2SnAs2 and a new modification of NaAs, J. Inorg. Gen. Chem./Z. Anorg. Allg. Chem. 636 (2010) 1691.
[25] Y. Park, D.C. Degroot, J. Schindler, C.R. Kannewurf, M.G. Kanatzidis, K2Cu5Te5, eine neuartige gemischtvalente Schichtverbindung mit metallischen Eigenschaften, Angew. Chem. 103 (1991) 1404–1407.
[26] S. Patel, A. Balchin, Structural studies of lithium intercalated titanium di-telluride, J. Mater. Sci. Lett. 4 (1985) 382–384.
[27] M. Oottil, New Structure Types Among Copper Chalcogenides by Mixing Tellurium with Sulfur or Selenium, University of Waterloo, 2010.
[28] W.-J. Huai, J.-N. Shen, H. Lin, L. Chen, L.-M. Wu, Electron-deficient telluride Cs3Cu20Te13 with sodalite-type network: syntheses, structures, and physical properties, Inorg. Chem. 53 (2014) 5575–5580.
[29] D. Jamwal, S.K. Mehta, Metal telluride nanomaterials: facile synthesis, properties and applications for third generation devices, Chemistry 4 (2019) 1943–1963.
[30] U. Shamraiz, A. Badshah, R.A. Hussain, M.A. Nadeem, S. Saba, Surfactant free fabrication of copper sulphide (CuS–Cu2S) nanoparticles from single source precursor for photocatalytic applications, J. Saudi Chem. Soc. 21 (2017) 390–398.
[31] U. Shamraiz, R.A. Hussain, A. Badshah, B. Raza, S. Saba, Functional metal sulfides and selenides for the removal of hazardous dyes from Water, J. Photochem. Photobiol., B 159 (2016) 33–41.
[32] W. Hussain, H. Malik, M.A. Khan, M.J. Iqbal, R.A. Hussain, R. Shoukat, Y. Khan, A. Badshah, M. Sulaman, H. Li, Comparative study of cobalt sulphides properties for photocatalytic and battery applications, Semicond. Sci. Technol. 34 (2019) 95015.
[33] T.S. Sunil Kumar Naik, S. Saravanan, K.N. Sri Saravana, U. Pratiush, P. C. Ramamurthy, A non-enzymatic urea sensor based on the nickel sulfide/graphene oxide modified glassy carbon electrode, Mater. Chem. Phys. 245 (2020) 122798.
[34] P.S. Prabhu, P. Kathirvel, H.B. Ramalingam, Synthesis of pure and Cr doped Zinc Sulfide nanoparticles for charge transport layers applications, Mater. Today: Proceedings 5 (2018) 16466–16471.
[35] W. Hussain, H. Malik, R.A. Hussain, H. Hussain, I.R. Green, S. Marwat, A. Bahadur, S. Iqbal, M.U. Farooq, H. Li, Synthesis of MnS from single-and multi-source precursors for photocatalytic and battery applications, J. Electron. Mater. 48 (2019) 2278–2288.
[36] W. Hussain, H. Malik, A. Bahadur, R. Hussain, M. Shoaib, S. Iqbal, H. Hussain, I. Green, A. Badshah, H. Li, Synthesis and characterization of CdS photocatalyst with different morphologies: visible light activated dyes degradation study, Kinet. Catal. 59 (2018) 710–719.
[37] H. Emadi, M. Salavati-Niasari, A. Sobhani, Synthesis of some transition metal (M: 25Mn, 27Co, 28Ni, 29Cu, 30Zn, 47Ag, 48Cd) sulfide nanostructures by hydrothermal method, Adv. Colloid Interface Sci. 246 (2017) 52–74.
[38] R.A. Hussain, A. Badshah, N. Haider, M.D. Khan, B. Lal, Effect of surfactants on the morphology of FeSe films fabricated from a single source precursor by aerosol assisted chemical vapour deposition, J. Chem. Sci. 127 (2015) 499–507.
[39] R.A. Hussain, A. Badshah, M.D. Khan, F. Ahmad, Morphological changes under the influence of surfactants of FeSe fabricated from single source precursor via AACVD

with mechanism and photocatalytic activity, Res. Develop. Mater. Sci. 9 (2019) 1–7.
[40] R.A. Hussain, A. Badshah, M.D. Khan, N. Haider, S.I. Khan, A. Shah, Comparative temperature and surfactants effect on the morphologies of FeSe thin films fabricated by AACVD from a single source precursor with mechanism and photocatalytic activity, Mater. Chem. Phys. 159 (2015) 152–158.
[41] R.A. Hussain, A. Badshah, S. Marwat, F. Yasmin, M.N. Tahir, Iron selenide nanoparticles coated on carbon nanotubes from single source ferrocene incorporated selenourea precursor for fuel cell and photocatalytic applications, J. Organomet. Chem. 769 (2014) 58–63.
[42] R.A. Hussain, A. Badshah, F. Yasmin, M.D. Khan, M.N. Tahir, Aerosol-assisted chemical vapour deposition for iron selenide thin films from single source ferrocene-incorporated selenourea precursor in the presence of surfactants, Aust. J. Chem. 68 (2015) 298–306.
[43] R.A. Hussain, A. Badshah, A. Younis, M.D. Khan, J. Akhtar, Iron selenide films by aerosol assisted chemical vapor deposition from single source organometallic precursor in the presence of surfactants, Thin Solid Films 567 (2014) 58–63.
[44] R.A. Hussain, I. Hussain, Manganese selenide: synthetic aspects and applications, J. Alloys Compd. 842 (2020) 155800.
[45] R.A. Hussain, I. Hussain, Use of surfactants to tailor the morphologies and crystalline phases of thin films via aerosol assisted chemical vapor deposition, J. Solid State Chem. (2020) 121429.
[46] A. Qin, Y. Fang, P. Tao, J. Zhang, C. Su, Silver telluride nanotubes prepared by the hydrothermal method, Inorg. Chem. 46 (2007) 7403–7409.
[47] R.E. Schaak, T.E. Mallouk, Prying apart Ruddlesden– Popper phases: exfoliation into sheets and nanotubes for assembly of perovskite thin films, Chem. Mater. 12 (2000) 3427–3434.
[48] Y. Xiong, Y. Xie, Z. Li, X. Li, S. Gao, Aqueous-solution growth of GaP and InP nanowires: a general route to phosphide, oxide, sulfide, and tungstate nanowires, Chemistry–A Eur. J. 10 (2004) 654–660.
[49] H. Fan, Y. Zhang, M. Zhang, X. Wang, Y. Qian, Glucose-assisted synthesis of CoTe nanotubes in situ templated by Te nanorods, Cryst, Growth Des 8 (2008) 2838–2841.
[50] E.-K. Kim, H.T. Bui, N.K. Shrestha, C.Y. Shin, S.A. Patil, S. Khadtare, C. Bathula, Y.-Y. Noh, S.-H. Han, An enhanced electrochemical energy conversion behavior of thermally treated thin film of 1-dimensional CoTe synthesized from aqueous solution at room temperature, Electrochim. Acta 260 (2018) 365–371.
[51] R. Shi, X. Liu, Y. Shi, R. Ma, B. Jia, H. Zhang, G. Qiu, Selective synthesis and magnetic properties of uniform CoTe and CoTe2 nanotubes, J. Mater. Chem. 20 (2010) 7634–7636.
[52] Z. Wang, F.-q. Wang, H. Chen, L. Zhu, H.-j. Yu, X.-y. Jian, Synthesis and characterization of Bi2Te3 nanotubes by a hydrothermal method, J. Alloys Compd. 492 (2010) L50–L53.
[53] Y. Deng, C.-W. Cui, N.-L. Zhang, T.-H. Ji, Q.-L. Yang, L. Guo, Fabrication of bismuth telluride nanotubes via a simple solvothermal process, Solid State Commun. 138 (2006) 111–113.
[54] Y. Cao, T. Zhu, X. Zhao, Thermoelectric Bi2Te3 nanotubes synthesized by low-temperature aqueous chemical method, J. Alloys Compd. 449 (2008) 109–112.
[55] J. Li, X. Tang, L. Song, Y. Zhu, Y. Qian, From Te nanotubes to CoTe2 nanotubes: a general strategy for the formation of 1D metal telluride nanostructures, J. Cryst. Growth 311 (2009) 4467–4472.
[56] L. Zhou, S. Yan, T. Lu, Y. Shi, J. Wang, F. Yang, Indium telluride nanotubes: solvothermal synthesis, growth mechanism, and properties, J. Solid State Chem. 211 (2014) 75–80.
[57] D. Pinisetty, D. Davis, E. Podlaha-Murphy, M. Murphy, A. Karki, D. Young, R. Devireddy, Characterization of electrodeposited bismuth–tellurium nanowires and nanotubes, Acta Mater. 59 (2011) 2455–2461.
[58] S. Kapoor, H. Ahmad, C.M. Julien, S.S. Islam, Synthesis of highly reproducible CdTe nanotubes on anodized alumina template and confinement study by photoluminescence and Raman spectroscopy, J. Alloys Compd. 809 (2019) 151765.
[59] A. Danine, K. Termentzidis, S. Schaefer, S. Li, W. Ensinger, C. Boulanger, D. Lacroix, N. Stein, Synthesis of bismuth telluride nanotubes and their simulated thermal properties, Superlattice. Microst. 122 (2018) 587–595.
[60] J. Ding, X. Wang, L.-H. Zhuo, B. Tang, Hierarchical assembly of CdTe nanotubes and nanowires at water–oil interface, J. Mater. Chem. 19 (2009) 3027–3032.
[61] Z. Chai, Z. Peng, C. Wang, H. Zhang, Synthesis of polycrystalline nanotubular Bi2Te3, Mater. Chem. Phys. 113 (2009) 664–669.
[62] B. Ketharachapalli, N.N. Pillala, R.K. Dash, Influence of the reducing agent on the formation and morphology of the bismuth telluride nanostructures by using template assisted chemical process: from nanowires to ultrathin nanotubes, J. Cryst. Growth 533 (2020) 125474.
[63] Y. Jiang, Y.-J. Zhu, L.-D. Chen, Microwave-assisted preparation of Bi2Te3 hollow nanospheres, Chem. Lett. 36 (2007) 382–383.
[64] Q. Yao, Y. Zhu, L. Chen, Z. Sun, X. Chen, Microwave-assisted synthesis and characterization of Bi2Te3 nanosheets and nanotubes, J. Alloys Compd. 481 (2009) 91–95.
[65] K.-R. Park, H.-B. Cho, Y.-H. Choa, Synthesis of ultra-long cadmium telluride nanotubes via combinational chemical transformation, Mater. Chem. Phys. 189 (2017) 64–69.
[66] K.-R. Park, H.-B. Cho, Y. Song, S. Kim, Y.-T. Kwon, S.H. Ryu, J.-H. Lim, W.-J. Lee, Y.-H. Choa, Large-scale synthesis of lead telluride (PbTe) nanotube-based nanocomposites with tunable morphology, crystallinity and thermoelectric properties, Appl. Sur. Sci. 436 (2018) 785–790.
[67] K.-R. Park, S. Kim, N.V. Myung, S.-O. Kang, Y.-H. Choa, Simple electrochemical synthesis of ultra-long silver telluride nanotubes, RSC Adv. 5 (2015) 29782–29785.
[68] G.-H. Dong, Y.-J. Zhu, L.-D. Chen, Sb 2 Te 3 nanostructures with various morphologies: rapid microwave solvothermal synthesis and Seebeck coefficients, CrystEngComm 13 (2011) 6811–6816.
[69] S. Zhang, D. Yang, M. Zhang, Y. Liu, T. Xu, J. Yang, Z.-Z. Yu, Synthesis of novel bimetallic nickel cobalt telluride nanotubes on nickel foam for high-performance hybrid supercapacitors, Inorg. Chem. Front. 7 (2020) 477–486.
[70] Z. Chai, H. Wang, Q. Suo, N. Wu, X. Wang, C. Wang, Thermoelectric metal tellurides with nanotubular structures synthesized by the Kirkendall effect and their reduced thermal conductivities, CrystEngComm 16 (2014) 3507–3514.
[71] H.-T. Zhu, J. Luo, J.-K. Liang, Synthesis of highly crystalline Bi 2Te3 nanotubes and their enhanced thermoelectric properties, J. Mater. Chem. 2 (2014) 12821–12826.
[72] K. Park, K. Ahn, J. Cha, S. Lee, S.I. Chae, S.-P. Cho, S. Ryee, J. Im, J. Lee, S.-D. Park, Extraordinary off-stoichiometric bismuth telluride for enhanced n-type thermoelectric power factor, J. Am. Chem. Soc. 138 (2016) 14458–14468.
[73] S. Liu, N. Peng, Y. Bai, H. Xu, D. Ma, F. Ma, K. Xu, General solvothermal approach to synthesize telluride nanotubes for thermoelectric applications, Dalton Trans. 46 (2017) 4174–4181.
[74] G. Zhang, Z.-A. Lan, L. Lin, S. Lin, X. Wang, Overall water splitting by Pt/gC3N4 photocatalysts without using sacrificial agents, Chem. Sci. 7 (2016) 3062–3066.
[75] J. Yu, L. Qi, M. Jaroniec, Hydrogen production by photocatalytic water splitting over Pt/TiO2 nanosheets with exposed (001) facets, J. Phys. Chem. C 114 (2010) 13118–13125.
[76] Q. Jia, A. Iwase, A. Kudo, BiVO 4–Ru/SrTiO 3: Rh composite Z-scheme photocatalyst for solar water splitting, Chem. Sci. 5 (2014) 1513–1519.
[77] T. Reier, Z. Pawolek, S. Cherevko, M. Bruns, T. Jones, D. Teschner, S.r. Selve, A. Bergmann, H.N. Nong, R. Schlögl, Molecular insight in structure and activity of highly efficient, low-Ir Ir–Ni oxide catalysts for electrochemical water splitting (OER), J. Am. Chem. Soc. 137 (2015) 13031–13040.
[78] D.K. Dogutan, R. McGuire Jr., D.G. Nocera, Electrocatalytic water oxidation by cobalt (III) hangman β-octafluoro corroles, J. Am. Chem. Soc. 133 (2011) 9178–9180.
[79] J. Masud, P.C. Ioannou, N. Levesanos, P. Kyritsis, M. Nath, A Molecular Ni-complex containing tetrahedral nickel selenide core as highly efficient electrocatalyst for water oxidation, ChemSusChem 9 (2016) 3128–3132.
[80] E. Smotkin, S. Cervera-March, A. Bard, A. Campion, M. Fox, T. Mallouk, S. Webber, J. White, Bipolar cadmium selenide/cobalt (II) sulfide semiconductor photoelectrode arrays for unassisted photolytic water splitting, J. Phys. Chem. 91 (1987) 6–8.
[81] M.E.C. Pascuzzi, A. Goryachev, J.P. Hofmann, E.J. Hensen, Mn promotion of rutile TiO2-RuO2 anodes for water oxidation in acidic media, Appl. Catal. B Environ. 261 (2020) 118225.
[82] Y. Gorlin, T.F. Jaramillo, A bifunctional nonprecious metal catalyst for oxygen reduction and water oxidation, J. Am. Chem. Soc. 132 (2010) 13612–13614.
[83] Q. Gao, C.Q. Huang, Y.M. Ju, M.R. Gao, J.W. Liu, D. An, C.H. Cui, Y.R. Zheng, W. X. Li, S.H. Yu, Phase-selective syntheses of cobalt telluride nanofleeces for efficient oxygen evolution catalysts, Angew. Chem. Int. Ed. 56 (2017) 7769–7773.
[84] I.G. McKendry, A.C. Thenuwara, J. Sun, H. Peng, J.P. Perdew, D.R. Strongin, M. J. Zdilla, Water oxidation catalyzed by cobalt oxide supported on the mattagamite phase of CoTe2, ACS Catal. 6 (2016) 7393–7397.
[85] Q. Liu, J. Jin, J. Zhang, NiCo2S4@ graphene as a bifunctional electrocatalyst for oxygen reduction and evolution reactions, ACS Appl. Mater. Interfaces 5 (2013) 5002–5008.
[86] H. Zhu, J. Zhang, R. Yanzhang, M. Du, Q. Wang, G. Gao, J. Wu, G. Wu, M. Zhang, B. Liu, When cubic cobalt sulfide meets layered molybdenum disulfide: a core–shell system toward synergetic electrocatalytic water splitting, Adv. Mater. 27 (2015) 4752–4759.
[87] Y. Li, L. Cao, L. Qiao, M. Zhou, Y. Yang, P. Xiao, Y. Zhang, Ni–Co sulfide nanowires on nickel foam with ultrahigh capacitance for asymmetric supercapacitors, J. Mater. Chem. 2 (2014) 6540–6548.
[88] R. Wang, X. Yan, Superior asymmetric supercapacitor based on Ni-Co oxide nanosheets and carbon nanorods, Sci. Rep. 4 (2014) 3712.
[89] B. Ye, M. Huang, L. Fan, J. Lin, J. Wu, Co ions doped NiTe electrode material for asymmetric supercapacitor application, J. Alloys Compd. 776 (2019) 993–1001.
[90] H. Chen, S. Chen, M. Fan, C. Li, D. Chen, G. Tian, K. Shu, Bimetallic nickel cobalt selenides: a new kind of electroactive material for high-power energy storage, J. Mater. Chem. 3 (2015) 23653–23659.
[91] L. Hou, Y. Shi, C. Wu, Y. Zhang, Y. Ma, X. Sun, J. Sun, X. Zhang, C. Yuan, Monodisperse metallic NiCoSe2 hollow sub-microspheres: formation process, intrinsic charge-storage mechanism, and appealing pseudocapacitance as highly conductive electrode for electrochemical supercapacitors, Adv. Funct. Mater. 28 (2018) 1705921.
[92] X. Song, C. Huang, Y. Qin, H. Li, H.C. Chen, Hierarchical hollow, sea-urchin-like and porous Ni 0.5 Co 0.5 Se 2 as advanced battery material for hybrid supercapacitors, J. Mater. Chem. 6 (2018) 16205–16212.
[93] L. Quan, T. Liu, M. Yi, Q. Chen, D. Cai, H. Zhan, Construction of hierarchical nickel cobalt selenide complex hollow spheres for pseudocapacitors with enhanced performance, Electrochim. Acta 281 (2018) 109–116.
[94] B. Ye, C. Gong, M. Huang, Y. Tu, X. Zheng, L. Fan, J. Lin, J. Wu, Improved performance of a CoTe//AC asymmetric supercapacitor using a redox additive aqueous electrolyte, RSC Adv. 8 (2018) 7997–8006.
[95] D. Galván, R. Rangel, E. Adem, Formation of MoTe2 nanotubes by electron irradiation, Fullerene Sci. Technol. 7 (1999) 421–426.